RSC Advances

ROYAL SOCIETY OF CHEMISTRY

www.rsc.org/advances

Journal Name

RSCPublishing

ARTICLE

Stabilization of Ni conductive filaments using NH_3 plasma treatment for electrochemical metallization memory

Cite this: DOI: 10.1039/xoxxoooooox

Received ooth January 2012,
Accepted ooth January 2012

DOI: 10.1039/xoxxoooooox

www.rsc.org/

Jingyu Park[1], Heeyoung Jeon[1], Hyunjung Kim[1], Woochool Jang[2], Hyoseok Song[2], Honggi Kim[1], Kunyoung Lee[2], and Hyeongtag Jeon[2,*]

In this study, NH_3 plasma treatment was utilized to enhance the resistive switching (RS) properties. Au/Ni/TaO_x/NiSi and Au/Ni/NH_3 plasma-treated TaO_x/NiSi resistance RAM (RRAM) devices were fabricated and the resistive switching (RS) properties of these devices were subsequently investigated. Both RRAM devices exhibited conventional electrochemical metallization memory (ECM) behaviors. However, the NH_3 plasma-treated samples exhibited an improved resistance distribution compared with that of non-treated samples due to the remaining Ni conductive filaments (CF), even following a RESET process. Additionally, superior retention properties longer than 10^4 s were observed due to the formation of stable Ni CFs. The formation of a defect-minimized TaON layer, observed via X-ray photoelectron spectroscopy (XPS), could be the source of stability for the Ni CFs, resulting in improved device behavior for the NH_3 plasma-treated samples.

Introduction

Conventional non-volatile memory (NVM) including NAND flash memory has experienced scaling limitations under the 20 nm technology node due to charge loss tolerance and cell to cell interference. Intensive research toward the development of next-generation NVM devices such as ferroelectric random access memory (FeRAM), magnetic RAM (MRAM), phase change RAM (PCRAM), and resistance RAM (RRAM), which have the potential to replace conventional NVM, is currently underway [1-3]. Among these potential solutions, RRAM has attracted particular attention due to its many advantages, including simple metal-insulator-metal (MIM) structure, fast switching speed, and excellent scalability, under the 10 nm technology node.

RRAM is categorized according to mechanism of resistive switching (RS) into interface type and conductive filament (CF) type [3, 4]. The RS of interface-type RRAM occurs at the interface between electrode and insulator. Many proposed models have been developed to explain interface-type RRAM, including the electrochemical migration of oxygen vacancies (V_o) [5], trapping of charge carriers [6], and Mott transition-induced carrier doping at the electrode/insulator interface [7]. On the other hand, filament-type RRAM is operated via the formation/rupture of CFs. Additionally, the composition of CFs can include V_o or an electrochemically active metal. The former type is known as valence change memory (VCM), whereas the latter is known as electrochemical metallization memory (ECM). The two RRAM types are dependent on the type of electrode material used in fabrication. When an electrochemically inert electrode such as Pt or W is both used as the top and bottom electrodes, the device operates via V_o CFs. On the other hand, when an electrochemically active metal is used as the top or bottom electrode with the other side being an electrochemically inert electrode, the device is operated via metal CFs. Ag and Cu metals are commonly used as electrochemically active metal materials [1, 2]. However, according to a recent study, Ni can also behave as an electrochemically active electrode due to its high charge mobility in insulator films [8].

Filament-type RRAM has superior characteristics compared to interface-type RRAM, such as large on/off ratios that enable multi-level cell operation and improved scalability due to independency within the device area [9]. Although many advantages of these devices have been mentioned, device reliability including retention is a huge problem that needs to be addressed [10, 11]. Toward solving this reliability issue, much research has been conducted, suggesting solutions such as insertion of a buffer layer [12], plasma

Journal Name RSCPublishing

ARTICLE

treatment [13], control of CF concentration [14], and adjusting switching conditions including SET pulses, RESET pulses, and current compliance [11].

In this study, Au/Ni/TaO_x/NiSi and Au/Ni/NH_3 plasma-treated TaO_x/NiSi devices were fabricated, and their reliability performances were investigated. The fabricated devices were operated via an ECM mechanism and showed large on/off ratios higher than 10^3. Additionally, NH_3 plasma-treated devices exhibited significantly improved device characteristics, including good resistance distributions and excellent retention, because the TaON layer stabilized the Ni CFs.

Experimental

A 2-inch boron-doped p-type Si (100) wafer with a measured resistivity in the range of 1 to 10 Ω·cm was used as the initial substrate. A 50-nm Ni film was deposited onto the Si (100) wafer via an e-beam evaporator. The Si wafer was subsequently cleaned with a dilute HF solution to remove the native oxide. The as-deposited Ni films were annealed at 500 °C for 1 minute via a rapid thermal annealing (RTA) process under vacuum to generate the NiSi films. Subsequently, a 20-nm TaO_x film was deposited onto the NiSi film via sputtering. Detailed deposition conditions are reported elsewhere [15]. The as-deposited TaO_x films were loaded into a remote plasma atomic layer deposition (RPALD) chamber prior to NH_3 plasma treatment. Inductively coupled plasma (ICP) with a radio frequency (rf) source power of 13.56 MHz was used to generate the NH_3 plasma. The NH_3 plasma treatment was carried out at 400 W for 2 minutes at room temperature (RT). Afterward, a 200-μm-diameter circular Ni film was deposited using a shadow mask via an e-beam evaporator. The Ni film thickness was 40 nm. A 10-nm Au film was likewise deposited using the same e-beam evaporator chamber and processes in order to prevent oxidation of the Ni film. As for the non-treated samples, Au/Ni/TaO_x films without NH_3 plasma treatment/NiSi RRAM devices were fabricated using the same methods.

Electrical properties of the Au/Ni/TaO_x/NiSi and Au/Ni/NH_3 plasma-treated TaO_x/NiSi RRAM devices were analyzed using an Agilent B1500A semiconductor parameter analyzer at RT. All devices were operated in DC voltage sweep mode. Voltage was applied to the Au/Ni top electrode, while the NiSi bottom electrode was grounded. During device operation, current compliance (CC) was set to 10 mA in order to prevent permanent breakdown. The binding energies of TaO_x films with and without NH_3 plasma treatment were also analyzed using X-ray photoelectron spectroscopy (XPS).

Results and discussion

Journal Name

RSCPublishing

ARTICLE

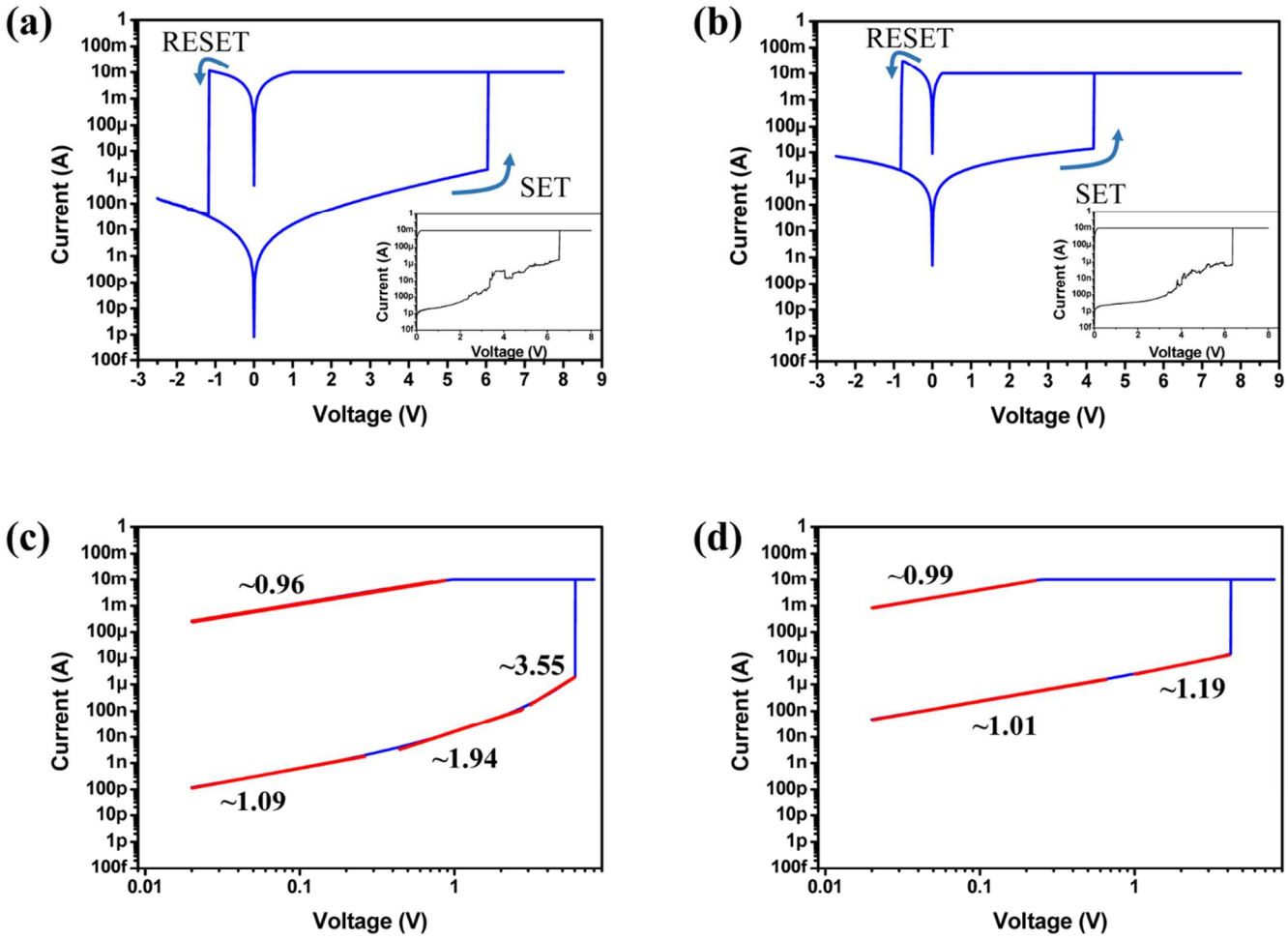

Figure 1 (Color online) The conventional I-V characteristics of (a) Au/Ni/TaO_x/NiSi and (b) Au/Ni/NH_3 plasma-treated TaO_x/NiSi RRAM devices (semi-log scale). The inset graphs in (a) and (b) reveal the initial forming stage of each device, respectively. The double log fitting results of (c) Au/Ni/TaO_x/NiSi and (d) Au/Ni/NH_3 plasma-treated TaO_x/NiSi RRAM devices.

Figure 1(a) and Figure 1(b) show typical current-voltage (I-V) graphs (semi-log scale) of Au/Ni/TaO_x/NiSi and Au/Ni/NH_3 plasma-treated TaO_x/NiSi RRAM devices, respectively. The inset graphs are of the initial forming stages for each device. The sweeping voltage was applied to the Ni top electrode (0 V → 8 V → 0 V → -2.5 V → 0 V) for both RRAM devices. For the Au/Ni/TaO_x/NiSi RRAM devices, the current increased abruptly at 6.04 V, SET operation [high resistance state (HRS) to low resistance state (LRS)], when an anode (Ni) bias was applied from 0 to 8 V. However, RESET operation (LRS to HRS) occurred at -1.18 V when a negative voltage was swept from 0 to -2.5 V. The I-V hysteresis of the Au/Ni/NH_3 plasma-treated TaO_x/NiSi devices is presented in Figure 1(b). Similar RS was observed for the NH_3 plasma-treated samples. SET operation was observed at 4.18 V and RESET operation occurred at -0.82 V; however, the device current was higher than that observed for the non-treated devices. Both devices exhibited conventional ECM characteristics such as large on/off ratios higher than 10^3 at a 0.1 V read voltage and abruptly changing currents at SET and RESET operations, which operated through formation/rupture of the metallic CFs.

In order to investigate the RS mechanism of each device, I-V graphs were re-plotted on a log-log scale. The LRS conduction mechanism of Au/Ni/TaO_x/NiSi RRAM devices exhibited ohmic behavior with a slope value of 0.96 in the overall voltage region, indicating that the device operated via formation of Ni CFs, as illustrated in Figure 1(c). However, the HRS conduction mechanism did not exhibit ohmic behavior, which contrasted with the LRS conduction mechanism. Charge transport was composed of three parts with different voltage

regions. The slope value was 1.09 in the low-voltage region, indicating ohmic behavior, and increased to 1.94 in the medium-voltage region, corresponding with Child's law. The slope value increased steeply in the high-voltage region. Therefore, the HRS conduction mechanism occurred through a conventional space charge-limited conduction (SCLC) mechanism [16]. Figure 1(d) reveals that the LRS conduction mechanism of Au/Ni/NH_3 plasma-treated TaO_x/NiSi RRAM devices involves ohmic behavior with a slope of 0.99 in all voltage regions. For the HRS, conduction mechanism was not clear because the slopes were 1.01 and 1.19 in the low- and high-voltage regions. The conduction mechanism could be dominated by tunneling gap because the HRS resistance value was higher than 12.9kΩ ($1/G_0 = h/2e^2$)[17]. The changing conduction mechanism was attributed to the NH_3 plasma treatment process.

Based on the I-V curve and the fitting results, the RS mechanism of Au/Ni/TaO_x/NiSi RRAM devices can be explained as follows. When a positive bias was applied to the Ni top electrode, Ni atoms were ionized to Ni ions (Ni^{z+} where z is 2 or 3) via charge transfer reactions and dissolved into the TaO_x films.

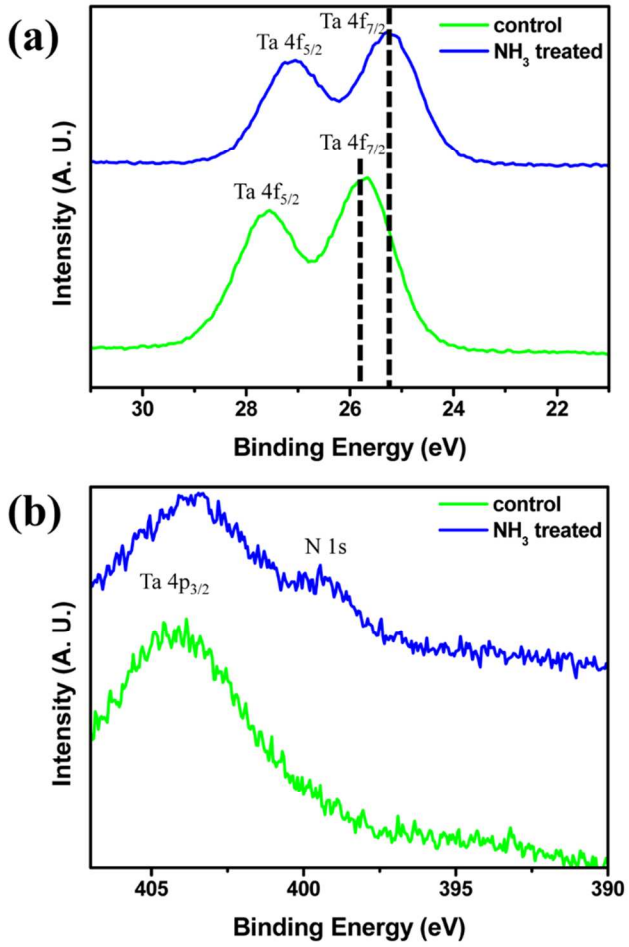

Figure 2 (Color online) (a) Tantalum 4f and (b) nitrogen 1s XPS results of TaO_x and NH_3 plasma-treated TaO_x films.

The Ni^{z+} ions subsequently migrated to the inert NiSi electrode via hopping mechanisms due to the applied electric field. When a Ni^{z+} ion reached the NiSi electrode, it was reduced, initiating the nucleation/growth of Ni CFs. Once Ni CFs connected the Ni electrode and NiSi electrode, the device resistance decreased (SET process). The device changed to HRS (RESET process) when a negative bias was applied to the Ni electrode because the Ni CFs were broken [2, 10, 18]. The Ni CFs were completely dissolved after the RESET process because the conduction mechanism of HRS was dominated by conventional SCLC processes. For the Au/Ni/NH_3 plasma-treated TaO_x/NiSi RRAM devices, the formation of Ni CFs occurred similarly as with non-treated devices during SET operation; however, the RESET process was different. Tunneling behavior was observed at the HRS, indicating that Ni CFs remained after the RESET process in NH_3 plasma-treated devices. Additionally, the source of the high HRS currents in NH_3 plasma-treated RRAM devices compared with non-treated devices was attributed to the remained Ni CFs. Similar results were observed in several previous reports of ECM devices [19-21].

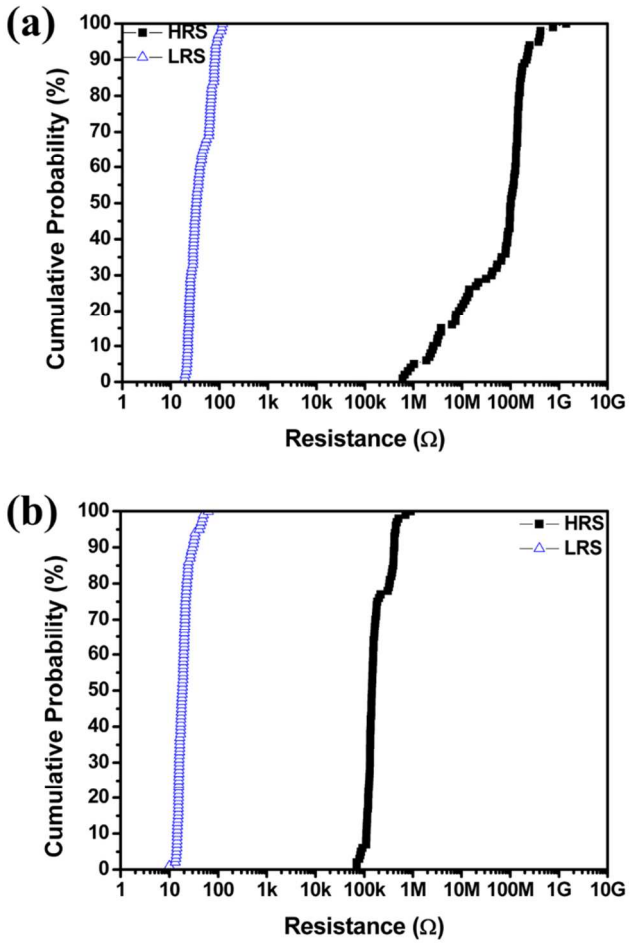

Figure 3 (Color online) The cumulative probability of (a) Au/Ni/TaO_x/NiSi and (b) Au/Ni/NH_3 plasma-treated TaO_x/NiSi RRAM devices.

In order to investigate the binding energy change of TaO_x films following NH_3 plasma treatment, XPS was employed. Figure 2(a) presents the XPS spectra of the Tantalum (Ta) 4f core level with and without NH_3 plasma treatment. The binding energy of the Ta 4f spectrum was calibrated using carbon contaminants in each sample at 284.5 eV due to the charging effect. The Ta $4f_{7/2}$ peak of the non-treated samples was observed at 25.75 eV. The

binding energy value was lower than the value observed for stoichiometric Ta_2O_5 (26.0 eV) [22], indicating that our as-deposited films consisted of Ta suboxide [22]. On the other hand, the Ta $4f_{7/2}$ binding energy of NH_3 plasma-treated TaO_x films was observed at 25.27 eV, which was lower than the binding energy measured for non-treated samples. The low binding energy was attributed to the incorporation of nitrogen within the TaO_x film and the formation of a TaON layer after NH_3 plasma treatment. These are natural phenomena as nitrogen possesses a lower electronegativity (3.04) than oxygen (3.44) [23]. In addition, nitrogen (N) 1s XPS spectra was measured to confirm the formation of TaON layer as shown in Figure 2 (b). Although Ta $4p_{3/2}$ spectra was overlapped with N 1s spectra, slight nitrogen spectra was observed only for NH_3 plasma treated sample. Therefore, it could be thought that TaON layer was formed after NH_3 plasma treatment.

Figures 3(a) and 3(b) demonstrate the cumulative probability of Au/Ni/TaO_x/NiSi and Au/Ni/NH_3 plasma-treated TaO_x/NiSi RRAM devices following 100 successive cycles at a read voltage of 0.1 V. For non-treated samples, the mean HRS and LRS resistance (μ_{HRS} and μ_{LRS}) values were 123 MΩ and 45 Ω, respectively. The HRS and LRS resistance standard deviations (σ_{HRS} and σ_{LRS}) were 171 MΩ and 24 Ω, respectively. Additionally, the HRS and LRS coefficients of variation (CV_{HRS} and CV_{LRS}) were 138% and 54%, respectively. However, in the case of the NH_3 plasma-treated samples, μ_{HRS} and μ_{LRS} were 205 kΩ and 20 Ω, while σ_{HRS} and σ_{LRS} were 141 kΩ and 8 Ω, respectively. The CV_{HRS} and CV_{LRS} values were 68% and 40%, respectively. Therefore, it is believed that the distribution of measured resistance values was significantly improved due to the NH_3 plasma treatment process.

In order to study the reliability of each RRAM device, a retention test was performed at RT. The HRS retention of Au/Ni/TaO_x/NiSi RRAM devices was stable for 5,000 seconds, as shown in Figure 4(a). However, the resistance of LRS increased abruptly after about 2,600 seconds due to dissolution of the Ni CFs. These results suggest that Ni CFs in non-treated samples are unstable even at RT. On the other hand, Au/Ni/NH_3 plasma-treated TaO_x/NiSi RRAM devices exhibited stable retention properties for 20,000 seconds for both HRS and LRS. Therefore, it is believed that the NH_3 plasma treatment process significantly enhances the stability of Ni CFs.

Figure 5(a) shows a schematic of the retention failure mechanism for Au/Ni/TaO_x/NiSi RRAM devices. The as-deposited TaO_x films yielded many defects because the TaO_x films consisted of non-stoichiometric suboxides, as shown in Figure 2 (a). The Ni CFs were readily oxidized to Ni ions and diffused to near the defect site owing to concentration gradient, especially near the top electrode, which resulted in an increased resistance, as shown in Figure 5(a). Stable Ni CFs were obtained by reducing defects near the top electrode. In a previous report, we successfully observed a much smaller defect density in the TaON layer than in TaO_x films due to strong N-O bonding using spectroscopy ellipsometry (SE) [24]. The formation of a TaON layer after NH_3 plasma treatment thereby reduced the density of defects. Therefore, diffusion of Ni ion from the Ni CFs is much decreased than non-treated device, resulting in stable retention characteristics, as shown in Figure 5(b). Additionally, the strong Ni CFs were not completely broken even after the RESET process, suggesting a source of the improved resistance distribution and HRS ohmic behavior of Au/Ni/NH_3 plasma-treated TaO_x/NiSi RRAM devices. If Ni CFs are present in films, the random formation of Ni CFs is suppressed because the electric field is focused on the tops of the remaining Ni CFs.

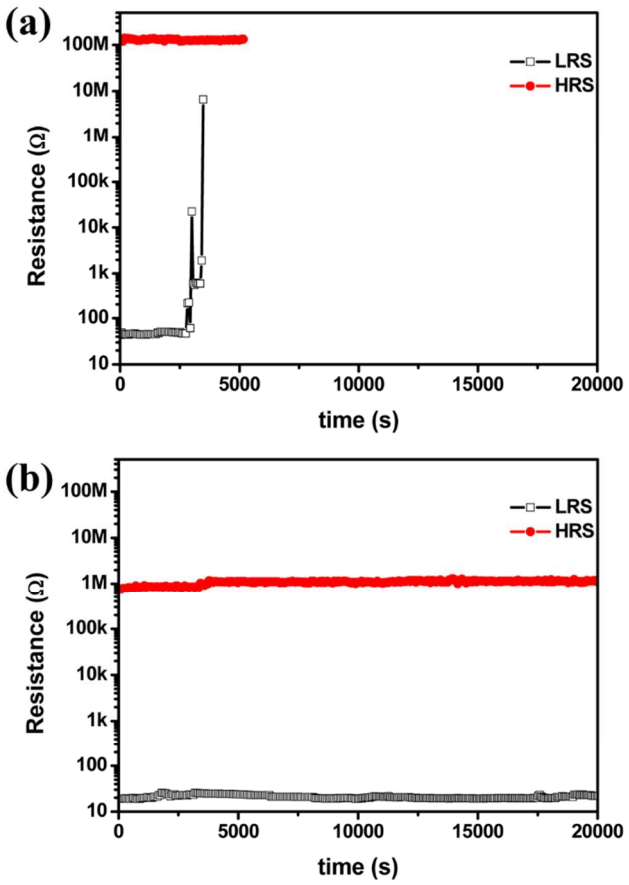

Figure 4 (Color online) The retention properties of (a) Au/Ni/TaO_x/NiSi and (b) Au/Ni/NH_3 plasma-treated TaO_x/NiSi RRAM devices.

Conclusions

The effect of NH_3 plasma treatment on RS properties of ECM devices was investigated. Au/Ni/TaO_x/NiSi and Au/Ni/NH_3 plasma-treated TaO_x/NiSi RRAM devices were fabricated as control and comparative specimen, respectively. The conduction mechanism of each device was extracted from the double logarithm I-V graph. The LRS conduction mechanism exhibited ohmic behavior for both devices. On the other hand, the HRS conduction mechanism was different for each device. The control device exhibited conventional SCLC conduction behavior, while the NH_3 plasma-treated device exhibited ohmic conduction behavior. The tunneling gap HRS conduction mechanism was attributed to the remaining Ni CFs after the RESET process. The remaining Ni CFs were the source of the improved resistance distribution because the electric field was focused on the tops of the remaining Ni CFs. Additionally, superior retention properties were observed due to the stable Ni CFs. The source of the strong Ni CFs in the NH_3 plasma-treated devices was the formation of a defect-free TaON layer on top

of the TaO_x films, which reduced the dissolution of Ni CFs via hopping mechanisms.

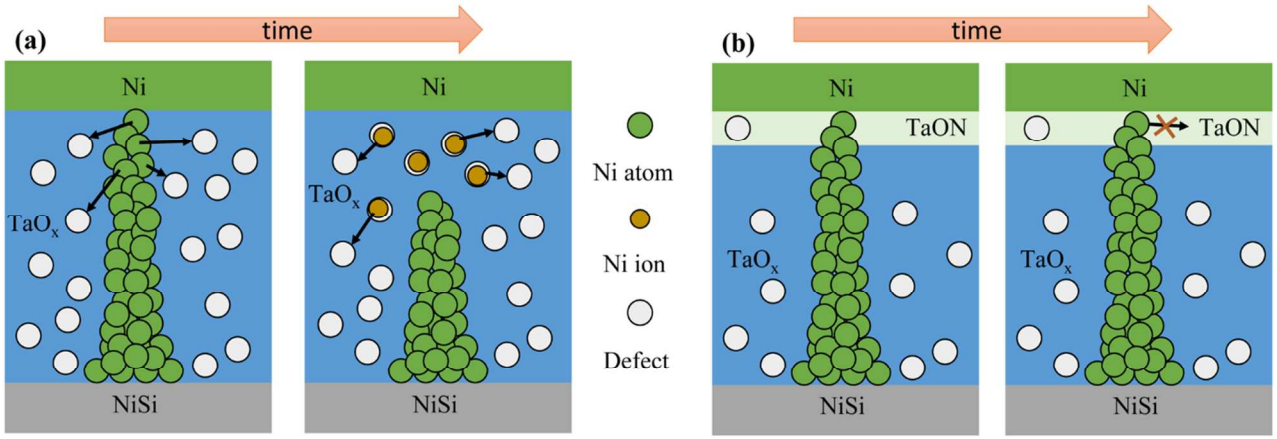

Figure 5 (Color online) (a) The retention failure mechanism of Au/Ni/TaO_x/NiSi RRAM devices and (b) the stabilization mechanism of Ni CFs for Au/Ni/NH_3 plasma-treated TaO_x/NiSi RRAM devices.

Acknowledgements

This work was supported by a National Research Foundation (NRF) of Korea grant funded by the Korean government (NRF-2014M3A7B4049367)

Notes and references

1 Department of Nano-scale Semiconductor Engineering, Hanyang University, Seoul, 133-791, Korea

2 Division of Materials Science and Engineering, Hanyang University, Seoul, 133-791, Korea

*Corresponding author. E-mail: hjeon@hanyang.ac.kr

1. R. Waser and M. Aono, *Nat Mater*, 2007, **6**, 833-840.
2. R. Waser, R. Dittmann, G. Staikov and K. Szot, *Adv Mater*, 2009, **21**, 2632-+.
3. A. Sawa, *Mater Today*, 2008, **11**, 28-36.
4. A. Prakash, D. Jana and S. Maikap, *Nanoscale Res Lett*, 2013, **8**.
5. S. Tsui, A. Baikalov, J. Cmaidalka, Y. Y. Sun, Y. Q. Wang, Y. Y. Xue, C. W. Chu, L. Chen and A. J. Jacobson, *Appl Phys Lett*, 2004, **85**, 317.
6. A. Sawa, T. Fujii, M. Kawasaki and Y. Tokura, *Appl Phys Lett*, 2004, **85**, 4073.
7. R. Fors, S. I. Khartsev and A. M. Grishin, *Phys Rev B*, 2005, **71**.
8. J. Sun, Q. Liu, H. Xie, X. Wu, F. Xu, T. Xu, S. Long, H. Lv, Y. Li, L. Sun and M. Liu, *Appl Phys Lett*, 2013, **102**, 053502.
9. J. Park, M. Jo, E. Bourim, J. Yoon, D. J. Seong, J. Lee, W. Lee and H. Hwang, *Ieee Electr Device L*, 2010, **31**, 485-487.
10. I. Valov, R. Waser, J. R. Jameson and M. N. Kozicki, *Nanotechnology*, 2011, **22**, 254003-254024.
11. H. B. Lv, X. X. Xu, H. T. Liu, R. Y. Liu, Q. Liu, W. Banerjee, H. T. Sun, S. B. Long, L. Li and M. Liu, *Sci Rep-Uk*, 2015, **5**.
12. B. Attarimashalkoubeh, A. Prakash, S. Lee, J. Song, J. Woo, S. Haque Misha, N. Tamanna and H. Hwang, *ECS Solid State Letters*, 2014, **3**, P120-P122.
13. C. Y. Liu, Y. H. Huang, J. Y. Ho and C. C. Huang, *J Phys D Appl Phys*, 2011, **44**.
14. J. Park, S. Jung, W. Lee, S. Kim, J. Shin, D. Lee, J. Woo and H. Hwang, *Ieee Electr Device L*, 2012, **33**, 646-648.
15. J. Park, H. Jeon, H. Kim, W. Jang, H. Seo and H. Jeon, *Rsc Adv*, 2014, **4**, 61064-61067.
16. Y. C. Yang, F. Pan, Q. Liu, M. Liu and F. Zeng, *Nano Lett*, 2009, **9**, 1636-1643.
17. S. B. Long, X. J. Lian, C. Cagli, X. Cartoixa, R. Rurali, E. Miranda, D. Jimenez, L. Perniola, M. Liu and J. Sune, *Appl Phys Lett*, 2013, **102**.
18. S. Menzel, S. Tappertzhofen, R. Waser and I. Valov, *Phys Chem Chem Phys*, 2013, **15**, 6945-6952.
19. D. Q. Liu, N. N. Wang, G. Wang, Z. Z. Shao, X. Zhu, C. Y. Zhang and H. F. Cheng, *Appl Phys Lett*, 2013, **102**.
20. S. Maikap, R. Panja and D. Jana, *Nanoscale Res Lett*, 2014, **9**.
21. X. L. Shao, J. S. Zhao, K. L. Zhang, R. Chen, K. Sun, C. J. Chen, K. Liu, L. W. Zhou, J. Y. Wang, C. M. Ma, K. J. Yoon and C. S. Hwang, *Acs Appl Mater Inter*, 2013, **5**, 11265-11270.
22. F. Kurnia, Hadiyawarman, C. U. Jung, R. Jung and C. Liu, *Phys Status Solidi-R*, 2011, **5**, 253-255.
23. S. Privitera, E. Rimini and R. Zonca, *Appl Phys Lett*, 2004, **85**, 3044-3046.
24. H. Jeon, J. Park, W. Jang, H. Kim, C. Kang, H. Song, H. Seo and H. Jeon, *Appl Phys Lett*, 2014, **104**.

